



In situ imaging of the conducting filament in a silicon oxide resistive switch

Jun Yao¹, Lin Zhong^{2,3}, Douglas Natelson^{2,4} & James M. Tour^{3,5}

SUBJECT AREAS:

ELECTRONIC MATERIALS
AND DEVICES

ELECTROCHEMISTRY

MATERIALS SCIENCE

IMAGING

¹Applied Physics Program through the Department of Bioengineering, Rice University, 6100 Main St., Houston, Texas 77005,

²Department of Electrical and Computer Engineering, Rice University, 6100 Main St., Houston, Texas 77005, ³Department of Computer Science, Rice University, 6100 Main St., Houston, Texas 77005, ⁴Department of Physics and Astronomy, Rice University, 6100 Main St., Houston, Texas 77005, ⁵Departments of Chemistry and Mechanical Engineering and Materials Science, Rice University, 6100 Main St., Houston, Texas 77005.

Received
30 September 2011

Accepted
19 December 2011

Published
31 January 2012

Correspondence and
requests for materials
should be addressed to
J.M.T. (tour@rice.edu)

The nature of the conducting filaments in many resistive switching systems has been elusive. Through *in situ* transmission electron microscopy, we image the real-time formation and evolution of the filament in a silicon oxide resistive switch. The electroforming process is revealed to involve the local enrichment of silicon from the silicon oxide matrix. Semi-metallic silicon nanocrystals with structural variations from the conventional diamond cubic form of silicon are observed, which likely accounts for the conduction in the filament. The growth and shrinkage of the silicon nanocrystals in response to different electrical stimuli show energetically viable transition processes in the silicon forms, offering evidence for the switching mechanism. The study here also provides insights into the electrical breakdown process in silicon oxide layers, which are ubiquitous in a host of electronic devices.

Understanding the mechanisms in resistive switching materials is essential for applications in future non-volatile memory and logic devices^{1–3}. When in the ON state, conduction in such systems can occur through a filament rather than the bulk channel. While filament confinement is considered advantageous⁴, it presents challenges in mechanistic probing. Surface conductance mapping provides useful information^{5–7}, yet the embedded nature of the filament makes further data difficult to obtain. Transmission electron microscopy (TEM) revealed structural and compositional details in the filaments^{8–10}. However, the isolation of the filament involved in this *ex situ* imaging^{8–10} is destructive and potentially alters it. Here we demonstrate the *in situ* imaging of the Si filament in a silicon oxide (SiO_x , $x \sim 2$) resistive switch. The Si nanocrystals are observed to be semi-metallic. The growth and shrinkage of the silicon nanocrystals offer insights into the switching mechanism. This could also have implications in a wide range of silicon oxide breakdown phenomena.

SiO_x resistive switching memory is attractive for its fully CMOS (complementary metal-oxide-semiconductor) compatible material composition and processing⁴. Two types of resistive switching memory have been constructed based on SiO_x . The first type belongs to the programmable metallization cell⁴, which relies on the formation and rupture of the metal filament injected from the electrode¹¹. It features bipolar switching behavior and is extrinsic to SiO_x with SiO_x merely serving as the passive solid electrolyte. The second type shows unipolar current-voltage (*I*-*V*) characteristics with the reset voltage larger than the set value⁹ (Fig. 1a). The filamentary switching was recently revealed to be the intrinsic property of SiO_x as it is electrode-independent^{9,12}. The study here focuses on this type of intrinsic resistive switching in SiO_x . While *ex situ* imaging revealed a silicon-rich switching site⁹, information regarding conduction and switching mechanisms was largely missing.

Through *in situ* TEM, we demonstrate the real-time imaging of the formation and evolution of the filament in a silicon oxide resistive switch. The electroforming process is shown to involve the local enrichment of silicon from the silicon oxide matrix. Semi-metallic silicon nanocrystals with structural variations from the conventional diamond cubic form of silicon are observed, which likely accounts for the conduction in the filament. The growth and shrinkage of the silicon nanocrystals in response to different electrical stimuli show energetically viable transition processes in the silicon forms, offering evidence for the switching mechanism. Since soft breakdown is involved in the electroforming process¹, the study here could also provide insights into the general electrical breakdown process in SiO_x , a material that plays a ubiquitous role in semiconductor electronics.

Results

Figs. 1b–d shows the schematics of the device design and setup for the *in situ* imaging. The imaging region consists of a SiO_x thin-walled structure covered by a layer of amorphous carbon ($\alpha\text{-C}$), which is connected to

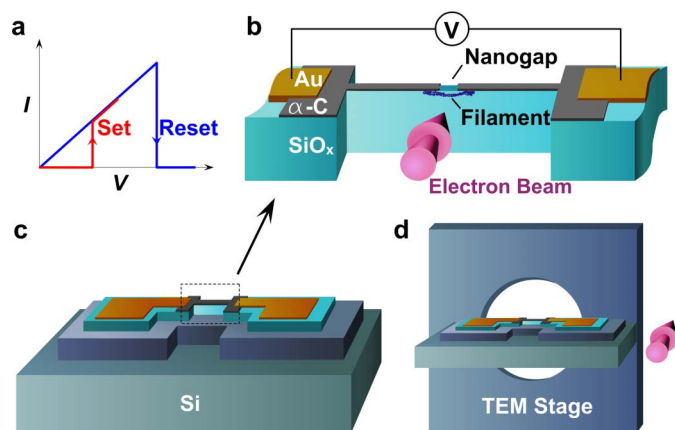


Figure 1 | *I-V* behaviors and general device embodiments. (a) Schematic of the unipolar switching in SiO_x , showing the typical set (red) and reset (blue) *I-V* curves (9). (b) Schematic of the SiO_x thin-walled structure for *in situ* TEM imaging. The switching region in SiO_x is localized by the nanogap generated in the $\alpha\text{-C}$ layer and imaged by TEM. (c) and (d) Schematics of the multi-stage structure and its arrangement with respect to the TEM stage. The pink arrows indicate the TEM electron beam imaging direction.

external electrical inputs (Fig. 1b). By electrical breakdown in the $\alpha\text{-C}$ layer, a disruption region or nanogap can be produced as we described previously in planar carbon-coated SiO_x devices¹². The broken ends of $\alpha\text{-C}$ layer then serve as the electrodes for the SiO_x in the nanogap region. The use of $\alpha\text{-C}$ as the electrode material eliminates possible extrinsic effects from metals¹¹, and the electrical breakdown-generated nanogap provides an easy method for the fabrication of closely spaced electrodes atop a thin-walled structure. The confinement from the nanogap pre-localizes the switching site so that it can be constantly monitored from before the electroforming or filament formation and throughout the experiment. During imaging, the electron beam from the TEM system travels perpendicularly across the SiO_x thin-walled structure. In this configuration, the SiO_x and the $\alpha\text{-C}$ layer are spatially separated in the imaging plane, minimizing possible interference from the electrode material. Practically, for the successful passage of the electron beam across the nanogap region, a multi-stage design with the SiO_x thin-walled structure is required (Fig. 1c). This multi-stage device is then vertically mounted on a home-built TEM stage (Supplementary Figs. S1, S2) that is capable of *in situ* electrical characterization (Fig. 1d). Note that while high vacuum environment ($\sim 10^{-8}$ Torr) is involved in the TEM system, the multi-stage devices also work in the regular vacuum environment ($\sim 10^{-5}$ Torr) in a probe station as was adopted for typical device testing^{9,12}. It shows the same resistive switching behaviors (Supplementary Fig. S3) with no SiO_x thin-wall thickness dependence, indicating the same switching mechanism intrinsic to SiO_x as reported previously.

Figs. 2a–d shows a series of scanning electron microscopy (SEM) images of the multi-stage device (see Supplementary Fig. S2 for fabrication details). The thickness of the SiO_x thin-walled structure is ~ 100 nm for the electron-beam transparency, and the length is $\leq 1 \mu\text{m}$ to reduce the resistance of the $\alpha\text{-C}$ electrodes (~ 20 nm thick). The successful imaging of the pristine structure by TEM is shown in Fig. 2e. After electrical breakdown in the $\alpha\text{-C}$ layer, a nanogap is generated in the $\alpha\text{-C}$ layer atop the SiO_x thin-walled structure (Fig. 2f).

Fig. 3 shows a series of high-resolution TEM images of the nanogap region (right panels) with respect to different *I-V* responses (left panels). Note that during the electrical characterization, the electron beam was temporarily blocked to exclude beam impact¹³. Immediately after the electrical breakdown in the $\alpha\text{-C}$ layer, a nanogap of ~ 15 nm is formed (Fig. 3a). Both the SiO_x at the nanogap

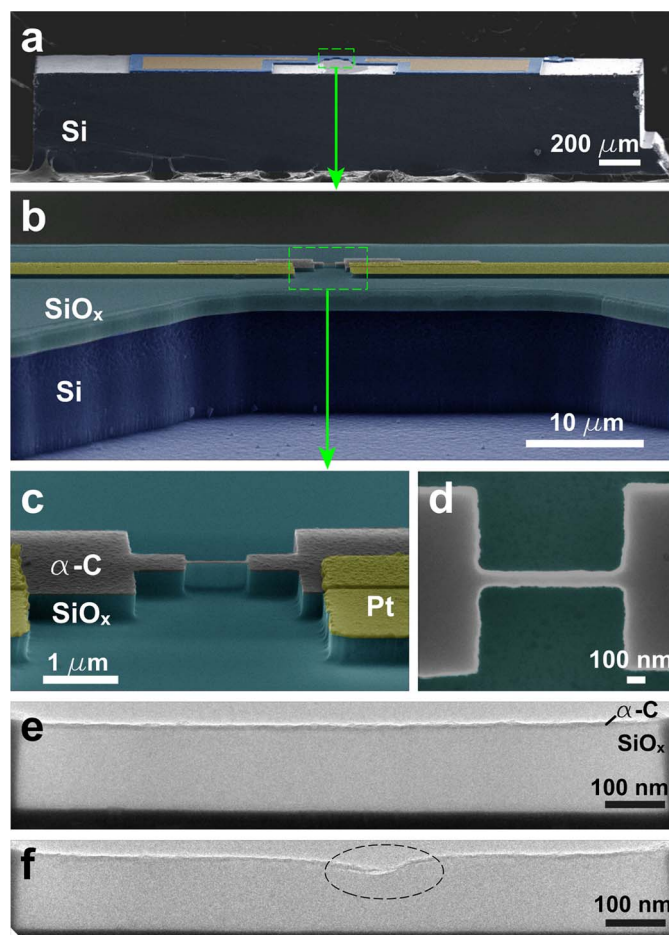


Figure 2 | SEM false-color images and TEM images of the electronic device. (a)–(c) Perspective SEM images of the multi-stage device for *in situ* imaging. (d) A top view of the SiO_x thin-walled structure. (e) Low-magnification TEM image of the SiO_x thin-walled structure with the $\alpha\text{-C}$ layer on top. (f) The same structure as in (e) with the $\alpha\text{-C}$ layer subjected to electrical breakdown. The circled region shows the nanogap in the $\alpha\text{-C}$ layer.

region and the SiO_x far from the nanogap show amorphous silica features. Because of the disruption in the $\alpha\text{-C}$ layer, the device shows little conduction during the subsequent voltage sweep, until at ~ 12 V the current suddenly increases (light grey curve in the plot of Fig. 3b). This conductance increase features the beginning of the electroforming process in SiO_x ⁹. The device is subsequently electroformed, showing the characteristic *I-V* curve featuring current increase (at ~ 5 V) and decrease (at ~ 10 V) that define the typical set and reset processes, respectively (grey curve). The device is set to the ON state (red curve). The immediate TEM imaging shows morphological changes at the nanogap region (Fig. 3b), as is often associated with the electroforming process^{8,9,14}. Specifically, out of the amorphous background, ~ 3 nm regions of nanocrystalline structure (based on the appearance of lattice fringes) appear at the nanogap (bounded region and inset in Fig. 3b). The apparent lattice spacing of the nanocrystal based on the fringes is distinct from that of the $\alpha\text{-C}$, indicating a different material form.

Due to the beam impact (see below), the formed ON and switching states degrade after imaging (light grey curve in Fig. 3c). A subsequent re-electroforming process is involved to set the device back to ON (grey and red curves). The immediate imaging shows growth in the nanocrystal (bounded region and inset in Fig. 3c). The partially degraded ON state after this imaging is compensated by a set process (red curve in Fig. 3d). For the subsequent voltage sweep to 14 V, a sudden decrease in the conductance occurs at ~ 12 V, featuring the

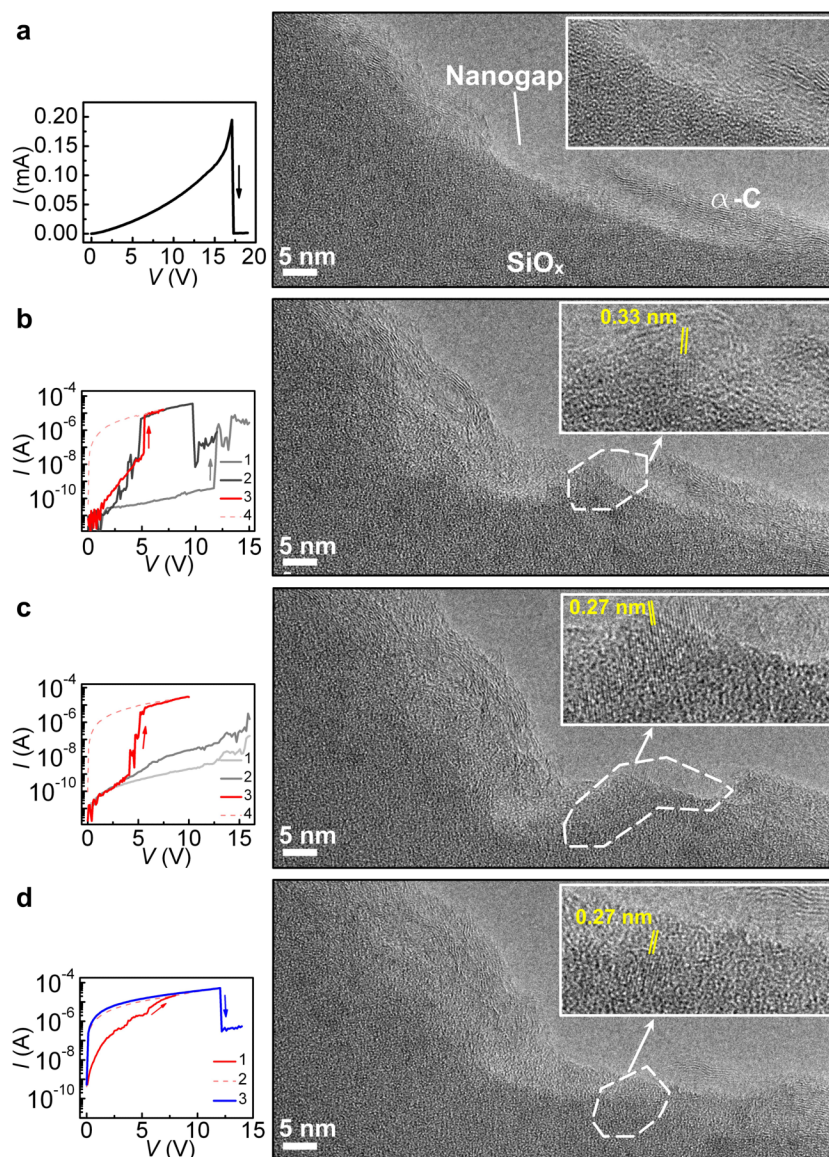


Figure 3 | High-resolution TEM images of the nanogap region (right panels) taken immediately after the electrical characterizations (left panels). (a) The electrical breakdown I - V curve in the α -C layer and the formed nanogap. The inset shows the enlarged nanogap region which shows only amorphous features. (b) The electroforming process in SiO_x with the state set to ON. The inset is an enlarged image of the circled region, showing nanocrystalline features. (c) A re-electroforming process in SiO_x after the imaging in (b), with the state set to ON. The inset shows the enlarged image of the circled region, showing the growth of the nanocrystal. (d) A reset process after the imaging performed in (c). The inset shows the enlarged image of the circled region, showing the shrinkage of size in the nanocrystal. The numbers in all the left-panel plots indicate the voltage-sweep orders.

typical reset process⁹. The immediate imaging shows prominent shrinkage in the size of the nanocrystal (bounded region and inset in Fig. 3d).

Discussion

The nanocrystalline structures were persistently observed only at the nanogap region in the switching devices, indicating their correlation with the electroforming and switching processes. Selected area electron diffraction shows that the crystalline structures are consistent with Si nanocrystals (NCs) and not silicon carbide (Supplementary Fig. S4). As SiO_x is the only source containing the Si element, the formation of the Si NCs shows that the energetically viable $\text{SiO}_x \rightarrow \text{Si}$ process is associated with the electroforming process. The *in situ* recording of this process also excludes the possibility of processing-induced formation during the filament isolation as was involved in *ex situ* imaging. This TEM imaging process was studied over four different devices (Supplementary Figs. S4, S5), all yielding similar information.

As the ON state shows largely metallic conduction¹⁵, questions arise regarding the composition of the conductor since conventional silicon is semiconducting. Lattice-spacing measurements and electron diffraction patterns from the Si NCs show evidence of structural deviation from the conventional diamond cubic Si-I phase. As shown in Fig. 4, the intersected lattice spacing of 0.33 and 0.32 nm with a nearly perpendicular angle is the feature of the Si-III phase¹⁶, which is semi-metallic¹⁷ and often associated with other conducting phases¹⁸. This indication can also be seen in Fig. 3; while the lattice spacing of 0.27 nm can be assigned to Si-I(200), Si-III(211) or Si-XII(11-2) faces, that of 0.33 nm (Fig. 3b) can only be associated with Si-III/Si-XII phases¹⁶. In particular, as Si-I(200) is the forbidden plane for diffraction¹⁹ and multiple scattering is considerably weakened at the nanoscale crystalline size, the strong signal of 0.27 nm⁻¹ in the diffraction patterns is further indication of the conducting Si-III/Si-XII phases²⁰ (Supplementary Figs. S4, S5). While these phase transitions in Si are typically induced by mechanical pressurization¹⁸, here it is

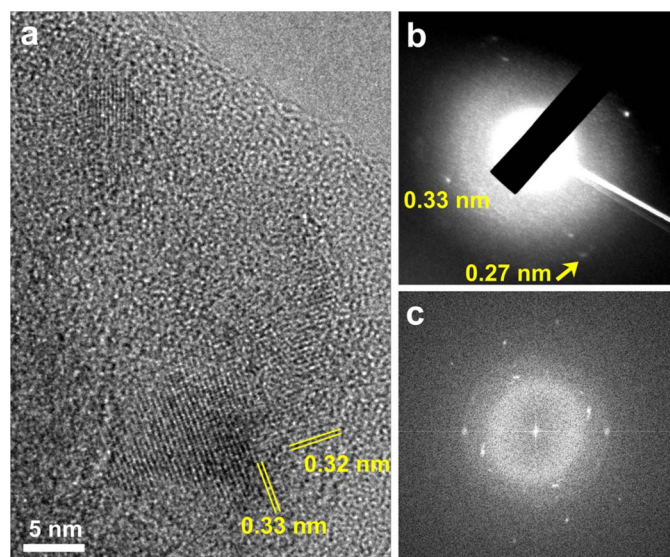


Figure 4 | TEM and diffraction patterns from a different device. (a) High-resolution TEM image of the nanogap region from another SiO_x switching device. (b) Selected-area diffraction pattern of the region shown in (a). (c) A fast Fourier transformed micrograph of the image shown in (a).

possible that the high electric field attained at the nanogap is inducing these phases. Indeed, the pressure induced by high electric field was revealed to induce structural distortion in silicon crystals²¹. The stability of the formed silicon phases at ambient environment^{17,18} also accounts for the electronically nonvolatile property in SiO_x resistive switching memory. Remarkably, the suppression of the electroforming and switching in SiO_x at low temperature^{9,15} coincides with the fact that the Si-III phase cannot be formed at liquid-nitrogen temperature²². Furthermore, the semi-metallic NCs suggest a rationale for failure to induce gating in three-terminal embodiments of these devices²³, which was originally proposed to be carbon switching²³ and later clarified as SiO_x -derived switching^{9,12}. Note that while the elementary composition of the Si filament was identified in our previous *ex situ* imaging study⁹, its structural variation from the conventional Si form was not revealed due to the absence of a diffraction pattern. This revelation could have been further hindered by the alteration of the Si forms during sample preparation by FIB in the *ex situ* imaging, as the ion beam can potentially induce phase transitions in the Si forms¹⁶.

From the devices studied, the filament in SiO_x is not in the form of a continuous single crystal across the nanogap, as seen in TiO_x switching systems⁸. Instead, discrete Si NCs form across the nanogap. Imaging such a filament is challenging, because of its 3-dimensional structure (e.g., having different depth profiles perpendicular to the imaging plane), different crystalline orientations, and the possibility of narrower filamentary constrictions (e.g. ≤ 1 nm) that are difficult to resolve from the environment. The growth of the Si NCs (Fig. 3c) indicates the general Si-rich nature along the nanogap in the electroformed device. This Si enrichment is also evidently correlated with the indentation and shrinkage of the volume at the nanogap region, likely a result of oxygen outgassing¹⁴. The shrinkage of the Si NCs with respect to the conductance drop (Fig. 3d) indicates the possible amorphization process. This is consistent with the thermally induced amorphization observed in the metallic Si phases^{18,20}, as the reset process in unipolar resistive switching is largely thermally stress-driven^{2,9,24}. In particular, resistance increase is associated with the amorphization process¹⁸. This provides a possible scenario for the filament rupture in the reset process.

We further take the electron-beam impact into consideration during the mechanistic interpretations. As mentioned above, the electron

beam from the TEM system tends to degrade the conduction and switching state in SiO_x . This does not indicate a charge-based mechanism though, as that was ruled out in the x-ray irradiation experiment and high temperature stability measurements⁹. In fact, knock-on structural change in Si can be readily induced by an electron beam at the imaging energy (200 KeV)²⁵, and the amorphization process can be induced^{16,26}. This accounts for the switching degradation after beam exposure (Fig. 3b) as structural changes along the entire filament are induced. While this is a further indication of structural change-induced conductance switching in the Si filament, it also implies that the structural transition needed for the switching can be subtle.

As was mentioned before, the SiO_x resistive switching system shows a larger reset voltage than the set value (i.e., $V_{\text{reset}} > V_{\text{set}}$)^{9,12,27}, which is different from typical unipolar systems that have $V_{\text{set}} > V_{\text{reset}}$ ^{1,2,28}. We suggest that the electric-field effect and thermal effect (by current local heating) are largely responsible for the set and reset processes, respectively, and that the competing process between the two effects results in this different behavior. The SiO_x resistive switching system features a lower ON-state conductance compared to other unipolar systems²⁸. As a result, no current compliance is needed in the set process to suppress the thermal reset effect. The thermally driven reset process is induced at a higher voltage V_{reset} ($V_{\text{reset}} > V_{\text{set}}$). Note that competition between the two processes persists in the region $V > V_{\text{reset}}$, with the thermal reset effect constantly overriding the set process driven by the field effect. This dynamic competition is evident from the large current fluctuations in the $V > V_{\text{reset}}$ region, which sometimes even shows transient ON-state fluctuations (Supplementary Fig. S3a). This competition also explains why during a backward sweep the system goes back into ON state below $V < V_{\text{reset}}$ (ref. 9,12,27), because the field is sufficient to set the system to ON at $V > V_{\text{set}}$ whereas the thermal effect is too weak to prevent this at $V < V_{\text{reset}}$. Note that while the thermal effect has been generally deemed responsible for the reset process in unipolar resistive switching systems^{1,30}, no direct observation has been made³⁰. Our *in situ* study provides further evidence and insights for this process.

In summary, the study here provides an overall picture of the intrinsic resistive switching in SiO_x . The electroforming is through the $\text{SiO}_x \rightarrow \text{Si}$ process with the semi-metallic Si state identified. The switching is indicated to be through the transition between the semi-metallic and amorphous Si forms. It also provides a general overview of electrical breakdown in silicon oxides. It should be noted that while a redox process was proposed to be responsible for the switching in our previous study⁹, the current study suggests switching based on structural transitions of the Si. The degradation of the resistive switching state to a nonswitchable metallic state (hard breakdown²⁹) in SiO_x is likely to be associated with the further aggregation of the metallic Si forms. The method described here can also be applied to other resistive switching materials for mechanistic investigation.

Methods

The multi-stage SiO_x thin-wall structure as shown in Fig. 2 is fabricated from a silicon wafer (thickness ~ 500 μm) capped with 2 μm thermal SiO_2 ($x \sim 2$) on top. The $\alpha\text{-C}$ layer was grown by chemical vapor deposition method at 900°C using C_2H_2 as precursor gas. Electron-beam lithography, photolithography and reactive ion etching steps were involved for the definition of the multi-stage SiO_x imaging structure (see Supplementary Information for more details). The fabricated structure was then mounted to a home-built TEM stage (Supplementary Figure S1) that is capable of electrical input, and electrically connected (through wire bonding) to an Agilent B1500 semiconductor parameter analyzer for the electrical characterizations. The imaging is carried out on a JEM-2100F TEM system with the beam energy at 200 KeV.

- Waser, R. & Aono, M. Nanoionics-based resistive switching memories. *Nat. Mater.* **6**, 833–840 (2007).
- Sawa, A. Resistive switching in transition metal oxides. *Materials Today* **11**, 28–36 (2008).



3. Lee, M.-J. *et al.* A fast, high-endurance and scalable non-volatile memory device made from asymmetric Ta_2O_5 - x / TaO_2 - x bilayer structures. *Nat. Mater.* **10**, 625–630 (2011).
4. Meijer, G. I. Who wins the nonvolatile memory race? *Science* **319**, 1625–1626 (2008).
5. Choi, B. J. *et al.* Resistive switching mechanism of TiO_2 thin films grown by atomic-layer deposition. *J. Appl. Phys.* **98**, 033715 (2005).
6. Szot, K., Speier, W., Bihlmayer, G. & Waser, R. Switching the electrical resistance of individual dislocations in single-crystalline SiTiO_3 . *Nat. Mater.* **5**, 312–320 (2006).
7. Liu, C. N., Stewart, D. R., Williams, R. S. & Bockrath, M. Direct observation of nanoscale centers in metal/molecule/metal structures. *Nano Lett.* **4**, 569–572 (2004).
8. Kwon, D. H. *et al.* Atomic structure of conducting nanofilaments in TiO_2 resistive switching memory. *Nat. Nanotechnol.* **5**, 148–153 (2010).
9. Yao, J., Sun, Z., Zhong, L., Natelson, D. & Tour, J. M. Resistive switches and memories from silicon oxide. *Nano Lett.* **10**, 4105–4110 (2010).
10. Yang, Y. C., Pan, F., Liu, Q., Liu, M. & Zeng, F. Fully room-temperature-fabricated nonvolatile resistive memory for ultrafast and high-density memory application. *Nano Lett.* **9**, 1636–1643 (2009).
11. Schindler, C., Thermaad, S. C., Waser, R. & Kozicki, M. N. Bipolar and unipolar resistive switching in Cu-doped SiO_2 . *IEEE Trans. Electron Devices* **54**, 2762–2768 (2007).
12. Yao, J. *et al.* Resistive switching in nanogap systems on SiO_2 substrates. *Small* **5**, 2910–2915 (2009).
13. Du, X.-W., Takeguchi, M., Tanaka, M. & Furuya, K. Formation of crystalline Si nanodots in SiO_2 films by electron irradiation. *Appl. Phys. Lett.* **82**, 1108 (2003).
14. Yang, J. J. *et al.* The mechanism of electroforming of metal oxide memristive switches. *Nanotechnol.* **20**, 215201 (2009).
15. Dearnaley, G., Stoneham, A. M. & Morgan, D. V. Electrical phenomena in amorphous oxide films. *Rep. Prog. Phys.* **33**, 1129 (1970).
16. Ge, D., Dominich, V. & Gogotsi, Y. High-resolution transmission electron microscopy study of metastable silicon phases produced by nanoindentation. *J. Appl. Phys.* **93**, 2418 (2003).
17. Besson, J. M., Mokhtari, E. H., Gonzalez, J. & Weill, G. Electrical properties of semimetallic silicon III and semiconductive silicon IV at ambient pressure. *Phys. Rev. Lett.* **59**, 473 (1987).
18. Ruffell, S., Sears, K., Bradby, J. E. & Williams, J. S. Room temperature writing of electrically conductive and insulating zones in silicon by nanoindentation. *Appl. Phys. Lett.* **98**, 052105 (2011).
19. Colella, R. & Merlini, A. A study of the (222) “forbidden” reflection in germanium and silicon. *Phys. Stat. Sol.* **18**, 157 (1966).
20. Ge, D., Domnich, V. & Gogotsi, Y. Thermal stability of metastable silicon phases produced by nanoindentation. *J. Appl. Phys.* **95**, 2725 (2004).
21. Aboyan, A. O. & Aghbalyan, S. G. Structural distortion of semiconducting silicon crystals caused by constant electric field. *Cryst. Res. Technol.* **45**, 140–144 (2010).
22. Khayyat, M. M., Banini, G. K., Hasko, D. G. & Chaudhri, M. M. Raman microscopy investigations of the structural phases transformation in crystalline and amorphous silicon due to indentation with a Vickers diamond at room temperature and at 77 K. *J. Phys. D: Appl. Phys.* **36**, 1300 (2003).
23. Li, Y., Sinitskii, A. & Tour, J. M. Electronic two-terminal bistable graphitic memories. *Nat. Mater.* **7**, 966–971 (2008).
24. J. C. Phillips. Internal stresses and formation of switchable nanowires at thin silica film edges. *J. Appl. Phys.* **109**, 034312 (2011).
25. Du, X.-W., Wang, B., Zhao, N. Q. & Furuya, F. Structure evolution of silicon nanocrystals under electron irradiation. *Scripta Materialia* **53**, 899–903 (2005).
26. Takeda, S. & Yamasaki, J. Amorphization in silicon by electron irradiation. *Phys. Rev. Lett.* **83**, 320 (1999).
27. Yao, J., Zhong, L., Natelson, D. & Tour, J. M. Silicon oxide: a non-innocent surface for molecular electronics and nanoelectronics studies. *J. Am. Chem. Soc.* **133**, 941–948 (2011).
28. Kim, D. C. *et al.* Electrical observations of filamentary conduction for the resistive memory switching in NiO films. *Appl. Phys. Lett.* **88**, 202102 (2006).
29. Dimaria, J. D., Cartier, E. & Arnold, D. Impact ionization, trap creation, degradation, and breakdown in silicon dioxide films on silicon. *J. Appl. Phys.* **73**, 3367 (1993).
30. Kim, K. M., Jeong, D. S. & Hwang, C. S. Nanofilamentary resistive switching in binary oxide system; a review on the present status and outlook. *Nanotechnology* **22**, 254002 (2011).

Acknowledgements

D. N. acknowledges the support of the David and Lucille Packard Foundation. L. Z. acknowledges support from the Texas Instruments Leadership University Fund and National Science Foundation Award No. 0720825. J. M. T. acknowledges support from the Army Research Office (# W911NF-08-C-0133, any opinions, findings and conclusions or recommendations expressed in this material are those of the author(s) and do not necessarily reflect the views of the U.S. Army Research Office) through the SBIR program administrated by PrivaTran, LLC. C. Kittrell aided in the design of the TEM probe device.

Author contributions

J. Y. designed and carried out the experiment, did the data analysis and wrote the paper. L. Z., D. N. and J. M. T. oversaw the project and edited the manuscript.

Additional information

Supplementary information accompanies this paper at <http://www.nature.com/scientificreports>

Competing financial interests: The authors declare no competing financial interests.

License: This work is licensed under a Creative Commons Attribution-NonCommercial-ShareAlike 3.0 Unported License. To view a copy of this license, visit <http://creativecommons.org/licenses/by-nc-sa/3.0/>

How to cite this article: Yao, J., Zhong, L., Natelson, D. & Tour, J.M. In situ imaging of the conducting filament in a silicon oxide resistive switch. *Sci. Rep.* **2**, 242; DOI:10.1038/srep00242 (2012).